POLSKA AKADEMIA NAUK

INSTYTUT MASZYN PRZEPŁYWOWYCH

TRANSACTIONS OF THE INSTITUTE OF FLUID-FLOW MACHINERY

PRACE INSTYTUTU MASZYN PRZEPŁYWOWYCH

104

GDAŃSK 1998

THE TRANSACTIONS OF THE INSTITUTE OF FLUID-FLOW MACHINERY

exist for the publication of theoretical and experimental investigations of all aspects of the mechanics and thermodynamics of fluid-flow with special reference to fluid-flow machines

*

PRACE INSTYTUTU MASZYN PRZEPŁYWOWYCH

poświęcone są publikacjom naukowym z zakresu teorii i badań doświadczalnych w dziedzinie mechaniki i termodynamiki przepływów, ze szczególnym uwzględnieniem problematyki maszyn przepływowych

Wydanie publikacji zostało dofinansowane przez PAN ze środków DOT uzyskanych z Komitetu Badań Naukowych

EDITORIAL OFFICE – REDAKCJA

Wydawnictwo Instytutu Maszyn Przepływowych
Polskiej Akademii Nauk
ul. Gen. Józefa Fiszera 14, 80-952 Gdańsk, skr. poczt. 621,
☎ (0-58) 341-12-71 wew. 141, fax: (0-58) 341-61-44,
e-mail: esli@imppan.imp.pg.gda.pl

ISSN 0079-3205

TRANSACTIONS OF THE INSTITUTE OF FLUID-FLOW MACHINERY

No. 104, 1998, 73-88

REINHARD WILLINGER[1], Hermann HASELBACHER[1]

Experimental and numerical investigation of the flow field in a linear turbine cascade including tip clearance effects

This paper presents details of an investigation of the three-dimensional flow field in a linear turbine cascade with the tip gap. The cascade geometry corresponds to the tip section of a moving blade row of a gas turbine of recent design. Five tip gap widths, including the case of zero gap width, have been investigated experimentally. A five-hole pressure probe was traversed immediately downstream of the trailing edge plane. The measurement results indicate a tip leakage vortex. Further work concerned the computation of the cascade flow field with a finite-element based Navier-Stokes solver. The k/ε-model was used to account for the turbulent behaviour of the flow. The inlet boundary conditions – mean and turbulence quantities – were adopted from the measured inlet flow field. The computational method is able to predict the essential features of the three-dimensional flow field qualitatively. The spatial location of the tip leakage vortex is predicted quite well, but its strength is underpredicted.

Nomenclature

c – blade chord length,
c_x – axial blade chord length,
C_p – static pressure coefficient,
C_{pt} – total pressure coefficient,
C_μ – constant in the k/ε-model,
h – blade channel height,
H_{12} – boundary layer shape factor,
i – number of the iteration step,
k – turbulent kinetic energy,
Ma – Mach number,
p – static pressure,
p_t – total pressure,
Re – Reynolds number,
s – blade spacing,
$\vec{u}$ – solution vector,
w – velocity,
x, y, z – global coordinates,
y', z – local coordinates,
y^+ – nondim. distance normal to the wall,
β – pitchwise flow angle, measured from the positive y'-direction,
β^+ – pitchwise flow angle, measured from the negative y'-direction,
γ – blade stagger angle, spanwise flow angle,
δ – characteristic lengths scale,
δ_{99} – boundary layer thickness,
δ_1 – boundary layer displacement thickness,
δ_2 – boundary layer momentum thickness,
ε – dissipation rate,
ξ' – local coordinate in chordwise direction,
ρ – density,
τ – tip gap width.

Subscripts

MS – midspan,
z – spanwise direction,

[1]Institute of Thermal Turbomachines and Powerplants, Vienna University of Technology, Getreidemarkt 9/313, A-1060 Vienna, Austria, Reinhard.Willinger@tuwien.ac.at

S –	secondary,	$2D$ –	two-dimensional,
t –	total,	1 –	inlet plane,
y –	circumferential (pitchwise) direction,	2 –	outlet plane.

1. Introduction

The design point performance and the off-design behaviour of axial turbomachines is strongly influenced by the flow in the tip gap region of the unshrouded rotor blades. For example, the tip leakage losses in an axial turbine can be as high as one third of the total loss [4]. Further, the stalling pressure rise capability of axial compressor stages is reduced, if the rotor tip gap width is increased [11]. Apart from the losses, the tip gap produces a flow underturning in the vicinity of the casing wall. The non-uniform distribution of the pitchwise flow angle along the blade span has to be taken into account for the design of the downstream flow path. This can be a stator blade row or a diffuser in the case of a last turbine stage. The performance of a last turbine stage is influenced by the interaction of the flow field at the rotor trailing edge plane and the pressure recovery of the diffuser. At increasing gap width, not only the tip leakage losses but also the kinetic energy of the casing boundary layer at the diffuser inlet increase. A wall jet is established which increases the diffuser pressure recovery which in turn lowers the back pressure of the upstream turbine stage. The decrease of the back pressure increases the specific work of the turbine. The aerodynamic interaction of a last gas turbine stage and an exhaust diffuser was investigated by Willinger [20]. The flow field downstream of the linear turbine cascade with various tip gap widths was measured with a five hole pressure probe. The diffuser flow field was investigated numerically with the appropriate inlet boundary conditions adopted from the cascade experiments. A theoretical model was derived to take into account the interaction of the two components. The efficiency of the turbine stage/diffuser combination is constant in the tip gap range usually employed. Apart from the experimental investigations on the cascade flow field, some numerical simulations have been performed. Results concerning the two dimensional flow and the secondary flow field in the cascade with zero tip gap width are summarized in [19,21]. This paper presents results of the three-dimensional flow field in the turbine cascade with the tip gap. The computational results are compared with own cascade measurements.

2. Experimental apparatus and procedures

2.1. Test cascade and test section

The geometry of the cascade under investigation is summarized in Fig. 1. The blade profile corresponds to the tip section of a moving blade row of a gas turbine of fairly recent design. Solidity, stagger and incidence angles differ slightly from the values of the tip section of the blade row in the engine. As a result, the blade in the experiment is somewhat more front-loaded than the actual rotor blade. The blades have constant chord and no twist and were milled from the solid aluminum blocks. At one end, the blades were bolted to the backplate of

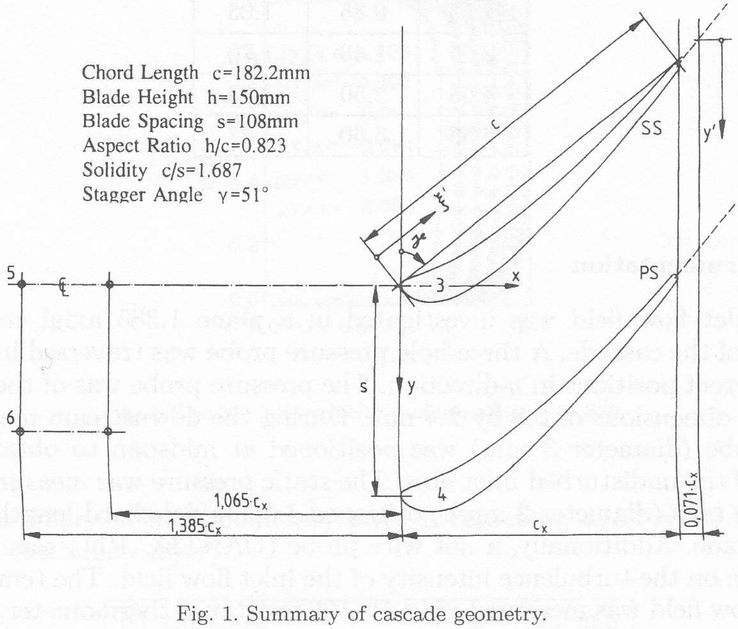

Fig. 1. Summary of cascade geometry.

the wind tunnel. Shims of different thicknesses were used to produce various tip gap widths. Following [3], the tip gap width of the moving blade row of a gas turbine varies from 1.5% to 2.5% of the chord. In the present investigation, this range is covered by four tip gap widths from 0.85% to 3.6% of the chord (Tab.1). Experimental and computational results presented in this paper are for a tip gap width of 3.6% of the chord. An exception is the blade pressure distribution. The experimental values are taken from measurements of Sjolander and Amrud [15] on a geometrically similar cascade with a tip gap width of 2.86% of the chord. Computed blade pressure distributions are also presented for this gap width. The cascade wind tunnel at the Institute of Thermal Turbomachines and Powerplants operates in the pressure mode. Air is supplied by an axial blower with variable inlet guide vanes. The test cascade, consisting of six blades, can be turned to adjust the inlet flow angle. In the present case, the inlet flow angle was fixed at $\beta_1 = 90^0$. End walls were attached to the leading edges of the first and the last blade of the cascade to guide the flow in the inlet section. Since the inlet flow field should show boundary layer parameters typical for a turbine blade row, there was no boundary layer bleeding.

Table 1. Summary of tip gap widths

τ [mm]	τ/c [%]	τ/h [%]
0	0	0
1.55	0.85	1.03
2.55	1.40	1.70
4.55	2.50	3.03
6.55	3.60	4.37

2.2. Instrumentation

The inlet flow field was investigated in a plane 1.385 axial chord lengths upstream of the cascade. A three-hole pressure probe was traversed in z-direction at six different positions in y-direction. The pressure probe was of the cobra type with head dimensions of 0.8 by 2.4 mm. During the downstream measurements, a Pitot tube (diameter 3 mm) was positioned at midspan to obtain the total pressure of the undisturbed inlet flow. The static pressure was measured by a row of pressure taps (diameter 2 mm) positioned 1.065 axial chord lengths upstream of the cascade. Additionally, a hot wire probe (DANTEC P11) was used to get information on the turbulence intensity of the inlet flow field. The temperature of the inlet flow field was measured via a Pt-100 resistance thermometer. A five hole pressure probe was traversed 0.071 axial chord lengths downstream of the trailing edge plane. This probe was of the conical type with a diameter of 3 mm and a total cone angle of 60^0. An exception was the traversing closest to the end wall. It was assumed that in this region the spanwise component of the flow can be neglected. So the three-hole probe was used for this traversing. Both probes were nulled in yaw. The static pressure at the end wall was measured by a row of pressure taps (diameter 2 mm). The 23 pitchwise and 11 spanwise traverses produced a grid of a total of 253 measuring points, with smaller spacings in the regions of supposedly high gradients of the flow quantities. These are the near wall region and the regions immediately behind the trailing edges. All pressure differences were measured with piezo-resistive pressure transducers (HONEYWELL) . The analogue pressure signals were converted to digital form via a HEWLETT-PACKARD HP 3852A data acquisition system. The system was controlled using LabWindows (NATIONAL INSTRUMENTS) on an IBM-compatible PC.

2.3. Operating conditions and inlet flow field

The magnitude of the undisturbed velocity at the inlet plane was about $w_{1,MS} = 32$ m/s. Since this corresponds to an upstream Mach number of approximately $Ma_{1,MS} = 0.1$, the flow field is essentially incompressible. The blade Reynolds number, defined with the undisturbed inlet velocity and the chord length, was $Re_{1,MS} = 3.63 \cdot 10^5$. The velocity distribution of the inlet flow field in the measuring plane 1.385 axial chord lengths upstream of the cascade is shown in Fig. 2.

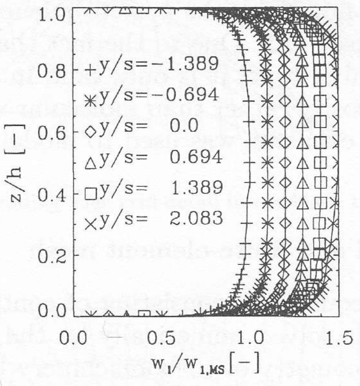

Fig. 2. Cascade inlet velocity profiles, $x/c_x = -1.385$.

Table 2. Summary of inlet boundary layer parameters, $x/c_x = -1.385$, $y/s = 0.694$, (b.l.=boundary layer)

b.l. thickness	$\delta_{99} = 22.9$ mm
b.l. displacement thickness	$\delta_1 = 2.0$ mm
b.l. momentum thickness	$\delta_2 = 1.5$ mm
b.l. shape factor	$H_{12} = 1.34$

The gap side end wall is located at $z/h = 0$, the blades are mounted at $z/h = 1.0$. The velocities are made dimensionless by the undisturbed upstream velocity $w_{1,MS}$. To improve the clarity of the illustration the curves obtained from the different traverses are staggered in the direction of the abscissa. The velocity distribution is symmetrical with respect to a plane $z/h = 0.5$, with a broad region of constant velocity magnitude. The end wall boundary layers are clearly visible. The parameters of the gap side end wall boundary layer at $y/s = 0.694$ are summarized in Tab. 2. The boundary layer shape factor of $H_{12} = 1.34$ is slightly lower than the typical value of $H_{12} = 1.4$ for turbulent boundary layers without pressure gradient. The turbulence intensity was about 5% in the region of constant velocity. The relatively high turbulence level in the freestream region is a consequence of a turbulence grid which is located in front of the nozzle of the cascade wind tunnel.

3. Numerical procedure

3.1. Governing equations

The numerical investigation was founded on the governing equations for steady three-dimensional incompressible turbulent flow. To take into account the turbulent characteristics of the flow field, the k/ε-turbulence model with the standard empirical constants was used [12]. Due to the fact that this turbulence model is of the high Reynolds number type, it is only valid in flow regions which are dominated by turbulent viscosity rather than molecular viscosity. The wall function method with special wall elements was used to model the flow in the vicinity of the solid walls [7].

3.2. Numerical method and finite-element mesh

The set of governing equations, consisting of continuity, momentum, k- and ε-transport equations, was solved numerically by the finite-element method [5]. Due to the complicated geometry of turbomachinery blade passages the grid generation is a complex task, especially if the radial tip gap is taken into account. In the past, the grid generation for cascades with tip gap was founded on the so-called „thin blade approximation" or „pinched tip approximation", since it allows the use of standard H-type grids [6,14] . The blade tip is cusped to zero and the grid lines of pressure and suction side coincide in the gap region. This approach is reasonable for thin blades (compressor) and is only suitable for modeling gross effects of the tip leakage flow since the tip geometry is not modeled correctly. Due to the fact that turbine blades have usually a higher ratio of thickness to chord, meshing techniques for the correct modeling of the blade tip are highly recommended. Recently, a variety of different meshing techniques for the correct modeling of the tip geometry have been published [2,9,10,13,18]. A comparison between the accuracy of the „thin blade approximation" and a correct modeling technique is given by Basson et al. [1].

The computational mesh in the present investigation is based on an H-0-H-grid in the blade-to-blade plane. An 0-grid was built around the blade and H-grids in the upstream and downstream regions. The blade-to-blade grid was stacked in the spanwise direction to produce a three-dimensional mesh. Fig. 3 shows the leading edge grid detail in the blade region. The space left in the 0-grid between the blade tip and the end wall was divided into two sub-domains formed by an 0-grid adjacent to the outer 0-grid described above and an inner H-grid (Fig. 4). Seven nodes are located between the blade tip and the end wall. The nodes in the tip gap are evenly spaced and all other nodes near the solid walls are stretched geometrically. The stacking of the blade-to-blade grid in the spanwise direction produced a three-dimensional finite-element mesh with 114275 nodes and 16590 elements, respectively (Fig. 5).

The thickness of the elements adjacent to the solid walls was adjusted to satisfy $10 \le y^+ \le 500$, with y^+ as the non-dimensional distance normal to the

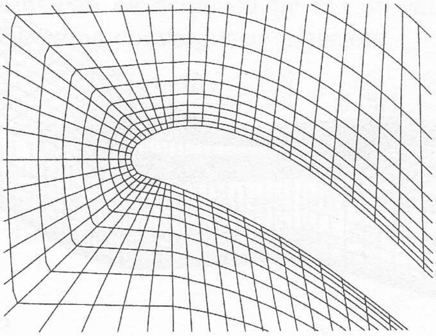

Fig. 3. Leading edge grid detail in the blade region.

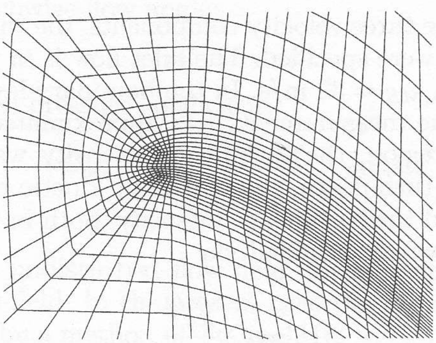

Fig. 4. Leading edge grid detail in the gap region.

wall. In the x-direction, the computation domain extends from the inlet plane ($x/c_x = -1.385$) to the outlet plane which is located approximately one axial chord length downstream of the cascade trailing edge plane. It is assumed that the tip clearance effects are noticeable only near the end wall and symmetry boundary conditions can be used at midspan. This assumption is supported by the results presented later in this paper. Thus, the computation domain is bounded by the end wall at $z/h = 0$ and the plane of symmetry at $z/h = 0.5$. In y-direction, the computation domain is bounded by two surfaces which are placed at an interval of one pitch (periodic boundaries). The angle between the periodic boundaries downstream of the cascade and the anticipated outlet flow direction results from the requirement that the elements should not be skewed too much. The computation domain was discretized by 27-nodal brick elements with triquadratic interpolation of the various flow quantities. An exception is the pressure degree of freedom the interpolation of which is of the trilinear type.

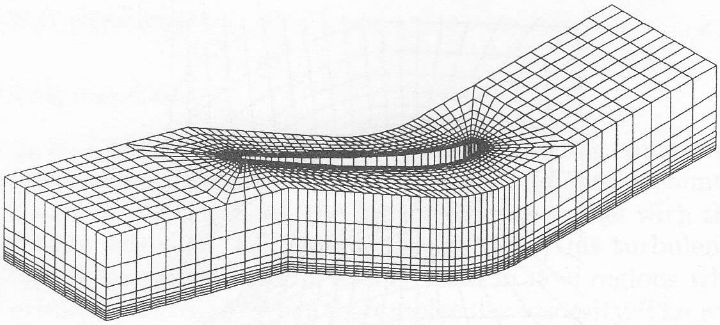

Fig. 5. Finite-element mesh.

3.3. Boundary conditions

At the inlet plane, the three velocity components, the turbulent kinetic energy and its dissipation rate were specified. The inlet flow is in the x-direction with a freestream velocity of $w_{1,MS} = 32$ m/s. In the boundary layer the velocity distribution obtained from the measurements was approximated by the 1/7th-power law. In the freestream region, the turbulence intensity was measured to about 5%. Assuming isotropic turbulence, the turbulent kinetic energy can be calculated from the velocity and the turbulence intensity, both in the freestream region. The rate of dissipation was determined via

$$\varepsilon_1 = C_\mu \frac{k_1^{3/2}}{\delta}. \tag{1}$$

The characteristic length scale δ was estimated to be 1% of the blade pitch [6]. No-slip boundary conditions were applied to the blade surface, to the blade tip and to the end wall. Symmetry boundary conditions at $z/h = 0.5$ ensure that there is no mass transport through the plane of symmetry and that all derivatives with respect to z are zero. The set of elliptic equations needs a boundary condition at the outlet plane as well. It is possible to specify either the velocity or the surface stress vector. At the outlet boundary, which is located far downstream of the cascade trailing edge plane, the surface stress vector was set to zero in a weighted sense. In the case of high Reynolds numbers, this so-called traction free condition is equivalent to a prescribed static pressure distribution. The derivatives of k and ε in the x-direction were set to zero at the outlet plane. To simulate a cascade with an infinite number of blades, cyclic boundary conditions for all variables were applied to the periodic boundaries.

3.4. Convergence and calculation time

The memory requirements and the calculation times are usually very high for the finite-element method in the case of three-dimensional flow computations. A substantial improvement can be achieved by the so called segregated solver [8]. This solver uses the following convergence criterion:

$$\frac{\|\vec{u}(i) - \vec{u}(i-1)\|}{\|\vec{u}(i)\|} \leq 0.001 \tag{2}$$

$\vec{u}(i)$ is the solution vector of the iteration step i. $\|.\|$ indicates the root mean square of a vector. Convergence was achieved after about 700 steps. The required CPU-time was about 40 hours on a DEC Alpha 8200 5/440.

4. Data reduction

The downstream plane at $x/c_x = 1.071$ comprises a rectangle of pitch by half span. The results are presented at this plane comprising the following local or pitchwise mass averaged quantities:
Lines of constant pitchwise flow angle:

$$\beta_2^+ = const. \tag{3}$$

Lines of constant total pressure coefficient:

$$C_{pt2} = \frac{p_{t2} - p_{t1,MS}}{\frac{1}{2}\rho w_{1,MS}^2} = const. \tag{4}$$

Secondary flow field:
The two-dimensional undisturbed flow field downstream of the cascade is often called a primary flow field. In the present case the direction of the primary flow field was determined by a method of Traupel [16] to $\bar{\beta}_{2,2D}^+ = 38.9^o$. This direction coincides closely with the tangent to the profile camber line at the trailing edge. The secondary flow field is then defined as the vectorial difference between the actual and the primary flow field

$$w_{2,Sy} = w_2 \cos\gamma_2 \sin(\beta_2^+ - \bar{\beta}_{2,2D}^+), \tag{5}$$

$$w_{2,Sz} = w_2 \sin\gamma_2. \tag{6}$$

Pitchwise mass averaged flow angle:

$$\bar{\beta}_2^+ = \frac{\int_0^s \beta_2^+ w_2 \cos\gamma_2 \sin\beta_2^+ \, dy'}{\int_0^s w_2 \cos\gamma_2 \sin\beta_2^+ \, dy'}. \tag{7}$$

Pitchwise mass averaged total pressure coefficient:

$$\bar{C}_{pt2} = \frac{\int_0^s C_{pt2} w_2 \cos\gamma_2 \sin\beta_2^+ \, dy'}{\int_0^s w_2 \cos\gamma_2 \sin\beta_2^+ \, dy}. \tag{8}$$

5. Results

5.1. Blade pressure distribution

The measured and computed pressure coefficients

$$C_p = \frac{p - p_1}{\frac{1}{2}\rho w_{1,MS}^2} \tag{9}$$

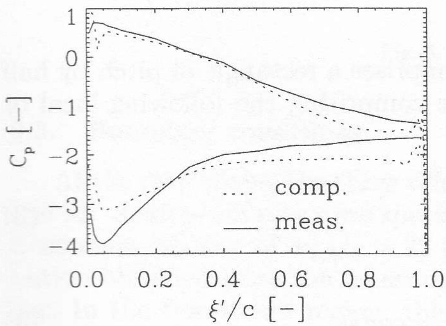

Fig. 6. Comparison between measured and computed pressure coefficients C_p at midspan ($z/h = 0.5$). Measured values are adopted from [15].

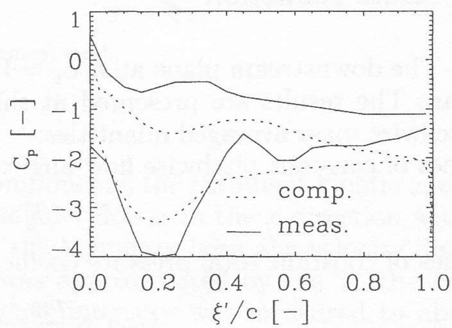

Fig. 7. Comparison between measured and computed pressure coefficients C_p at the blade tip ($z = \tau$). Measured values are adopted from [15].

at midspan ($z/h = 0.5$) and at the blade tip ($z = \tau$) are plotted in Fig. 6 and 7, respectively. The measured values are adopted from Sjolander and Amrud [15]. The authors investigated a geometrically similar cascade at a blade Reynolds number of $Re_{1,MS} = 4.3 \cdot 10^5$. As mentioned, the blade pressure distributions are given for a gap width of $\tau/c = 2.86\%$. This is somewhat lower than the gap width of $\tau/c = 3.6\%$, for which the main part of the results is presented. The agreement between measured and computed blade pressure distribution at midspan is quite good (Fig. 6). Some differences are visible in the stagnation region. On one hand, the resolution of steep gradients is limited by the finite number of pressure taps. On the other hand, the wall function method, which requires quasi-one-dimensional flow, fails in the stagnation region. Further differences are apparent at the suction side. The pressure coefficients are overpredicted in the minimum pressure region and underpredicted at the rear. Generally, the agreement between measured and computed blade pressure distribution is not so good at the blade tip (Fig. 7) . The minimum pressure peak on the suction side at $\xi'/c = 0.2$ is underpredicted by the computation. This indicates that the strength of the computed tip leakage vortex is weaker than the measured one. The second suction peak at $\xi'/c = 0.6$ was attributed by Sjolander and Amrud [15] to a second tip leakage vortex. The computation supplies only one tip leakage vortex, as can be seen in the pressure distribution. On the pressure side, the pressure coefficients are computed generally too low. The gradients near the pressure side corner of the blade tip are very steep. So the pressure taps, which are located a small distance away from the blade tip, experience a somewhat higher pressure compared to the blade tip.

5.2. Local quantities

Fig. 8 and 9 show the measured and computed pitchwise flow angles β_2^+. The outlet flow angle of the two-dimensional undisturbed cascade flow was estimated to $\bar{\beta}^+_{2,2D} = 38.9^o$. This flow angle was verified in the freestream region by the present measurement as well as by the computation. The tip leakage vortex is responsible for the underturning near the end wall. The highest measured pitchwise flow angles are about $\beta_2^+ = 75^o$. The highest computed pitchwise flow angles are somewhat lower and are about $\beta_2^+ = 70^o$. The minimum measured flow angle in the overturning region is about $\beta_2^+ = 25^o$, compared to the measured value of about $\beta_2^+ = 35^o$.

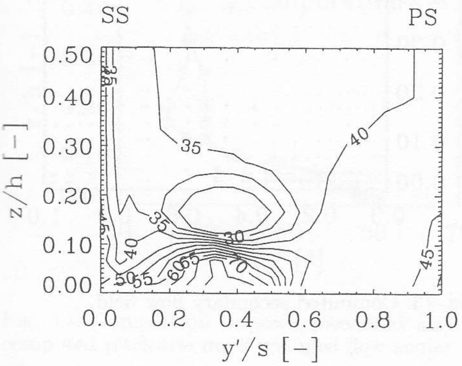

Fig. 8. Measured pitchwise flow angles $\beta_2^+ =$ *const.*

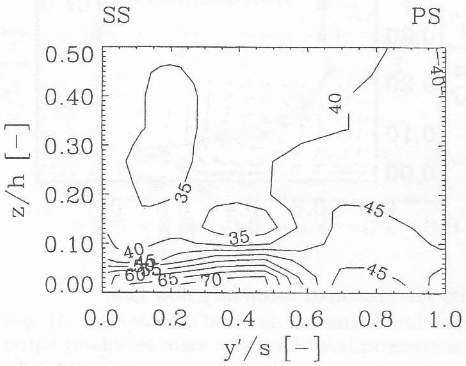

Fig. 9. Computed pitchwise flow angles $\beta_2^+ =$ *const.*

The quality of the energy exchange in the turbine cascade is characterized by the total pressure coefficient evaluated immediately downstream of the trailing edges. The measured and computed total pressure coefficients in the plane $x/c_x = 1.071$ are plotted in Fig. 10 and 11, respectively. The inviscid region of the downstream flow field is characterized by a zero total pressure coefficient. In the region of the two-dimensional flow ($z/h \geq 0.3$) the total pressure losses are concentrated in the wake regions. The experiment as well as the computation indicates a thicker suction side boundary layer compared to that on the pressure side. However, the computation gives substantially thicker blade boundary layers. Especially the thickness of the computed suction side boundary layer is very high. Another high loss region is located in the corner between the blade suction side and the end wall at $y'/s = 0.35$ and $z/h = 0.1$, respectively. The tip leakage vortex is responsible for this high loss region.

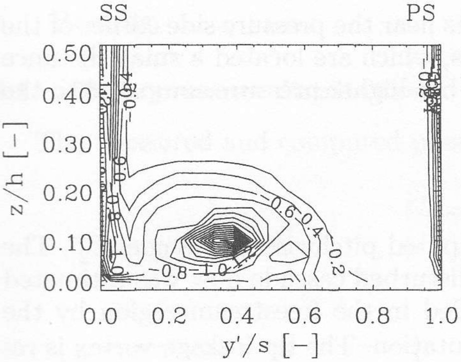

Fig. 10. Measured total pressure coefficients $C_{pt2} = const.$

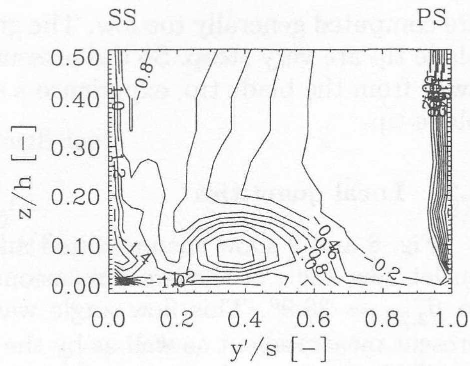

Fig. 11. Computed total pressure coefficients $C_{pt2} = const.$

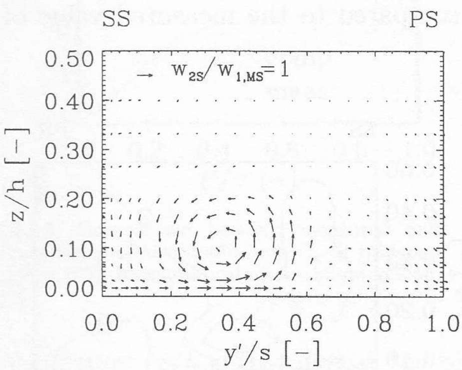

Fig. 12. Measured secondary flow field.

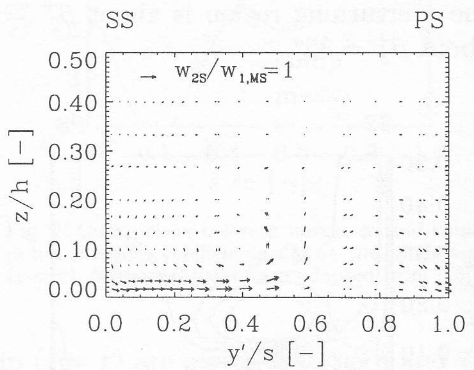

Fig. 13. Computed secondary flow field.

For further visualization of the downstream flow field, measured and computed secondary flow fields are given in Fig. 12 and 13, respectively. The measured tip leakage vortex shows an axisymmetric structure in the plane $x/c_x = 1.071$. The measurement as well as the computation gives approximately the same location of the vortex center. However, the computed tip leakage vortex shows a highly non-symmetrical structure. The underturning near the end wall is much stronger than the overturning on the opposite side of the center of the vortex.

5.3. Pitchwise mass averaged quantities

In Fig. 14, the pitchwise mass averaged flow angles $\bar{\beta}_2^+$ are plotted as a function of the spanwise coordinate. In the region $z/h \geq 0.3$, the estimated flow angle $\bar{\beta}_{2,2D}^+ = 38.9^o$ is verified by the present measurement and the computation. The measurement as well as the computation gives a maximum underturning of about 20^o in the end wall region. Moving away from the end wall, the measurement gives a maximum overturning of about 3^o. No overturning is supplied by the computation. This result was expected taking the non-axisymmetric structure of the computed tip leakage vortex into account. Fig. 15 shows the pitchwise mass averaged total pressure coefficients $\bar{C}_{pt2}$ as a function of the spanwise coordinate. In the region $z/h > 0.3$, the measured total pressure coefficient is rather constant. The associated loss is called the profile loss. Toward the end wall, the total pressure loss increases (decreasing total pressure coefficient) and reaches a peak value at $z/h = 0.1$. This is the location of the center of the tip leakage vortex in spanwise direction. As expected from the lines of constant total pressure coefficients (Fig. 11), the computed losses in the region $z/h \geq 0.3$ are clearly too high. This discrepancy is attributed to the excessive thickness of the computed suction side boundary layer. In the tip leakage vortex region, the measured and computed total pressure losses coincide quite well, although the peak of the computed loss distribution is shifted nearer toward the end wall. However, this correspondence is accidental, since the strength of the tip leakage vortex is computed too weak.

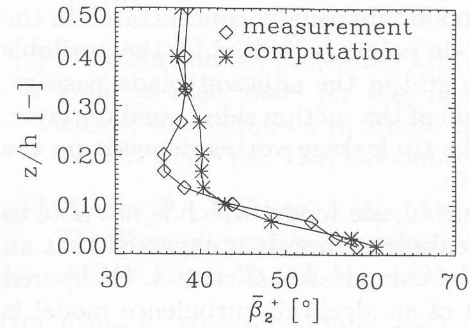

Fig. 14. Comparison between measured and computed pitchwise mass averaged flow angles $\bar{\beta}_2^+$.

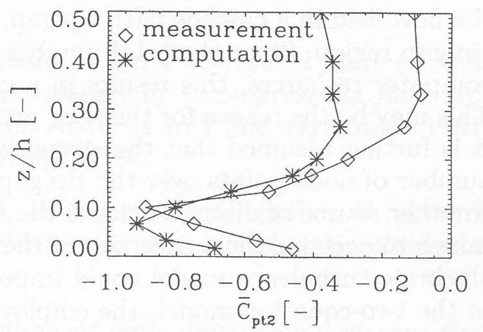

Fig. 15. Comparison between measured and computed pitchwise mass averaged total pressure coefficients $\bar{C}_{pt2}$.

6. Conclusions

The steady three-dimensional incompressible turbulent flow field in a linear turbine cascade with a tip gap of 3.6% of the chord was investigated numerically by a finite-element based Navier-Stokes solver. The k/ε- model was used to account for the turbulent behaviour of the flow field. For the verification of the computation, the flow field immediately downstream of the trailing edge plane was measured in the cascade wind tunnel. The finite-element method employs an embedded mesh technique for the meshing of the tip gap region in a very straightforward manner. The computational method is able to predict the essential features of the three-dimensional flow field only qualitatively. When the geometry of the cascade is changed from the simple two-dimensional case and the cascade

without tip gap to the cascade with tip gap, the complexity of the flow field increases dramatically. At the same time, the accuracy of the computational results decreases. In the present case, the suction side blade boundary layer is computed substantially too high, which results in an overprediction of the profile loss. The location of the tip leakage vortex is computed quite good, but its strength is predicted too weak. So the correspondence of the measured and the predicted total pressure loss in the vortex region is accidental. It is assumed that the following reasons are responsible for the inability of the computational method to predict the flow field correctly:
The main reason is the so-called numerical diffusion of the Navier-Stokes code. An improvement is achieved by a reduction of the streamline upwinding, as it was shown by Trenker [17] for the two-dimensional flow in a compressor cascade. However, a certain degree of upwinding is necessary to guarantee the numerical stability of the iteration process.
Further improvement is achieved when the number of nodes is increased, as it was demonstrated in the two-dimensional case [19]. In the case of the computation of the flow field in a cascade with tip gap, the nodes are usually concentrated in the tip gap region. Since the total number of node points is limited by the available computer resources, this results in a coarse grid in the adjacent blade passage. This may be the reason for the poor prediction of the suction side boundary layer. It is further assumed that the strength of the tip leakage vortex depends on the number of node points over the tip gap width.
Another source of discrepancies is the k/ε-turbulence model which is not able to take into account the anisotropy of the tip leakage vortex. It is expected that an algebraic turbulence model could improve the computational results. Compared to the two-equation model, the employment of an algebraic turbulence model is further suggested by the reduced computational costs. Last but not least, the laminar/turbulent transition is totally neglected by the numerical method.
An improvement of the computational results is desirable, since the flow field at the trailing edge plane supplies the inlet boundary conditions for the downstream diffuser.

Manuscript received in April 1998

References

[1] Basson A. H., Kunz R. F., Lakshminarayana B.: *Grid generation for three-dimensional turbomachinery geometries including tip clearance*, AIAA Journal of Propulsion and Power, Vol. 9, No. 1, January - February 1993, 59-66.

[2] Basson A., Lakshminarayana B.: *Numerical simulation of tip clearance effects in turbomachinery*, ASME Journal of Turbomachinery, Vol. 117, July 1995, 348-359.

[3] Bindon J. P. : *Pressure distributions in the tip clearance region of an unshrouded axial turbine as affecting the problem of tip burnout*, ASME Paper 87-GT-230, 1987.

[4] Denton J. H.: *Loss mechanisms in turbomachines*, ASME Journal of Turbomachinery, Vol. 115, October 1993, 621-656.

[5] FD1: FIDAP-Users Manual. Rev. 7.0, Fluid Dynamics International Inc., Evanston, 1993.

[6] Hah C.: *A numerical modeling of endwall and tip-clearance flow of an isolated compressor rotor*, ASME Journal of Engineering for Gas Turbines and Power, Vol. 108, January 1986, 15-21.

[7] Haroutunian V., Engelman M.S.: *On modeling wall-bound turbulent flows using specialized near-wall finite elements and the standard $k-\varepsilon$ turbulence model*, First ASME/JSME Fluids Engineering Conference, FED-117, 1991, 97-105.

[8] Haroutunian V., Engelman M.S., Hasbani I.: *Three segregated finite element solution algorithms for the numerical solution of incompressible flow problems*, in: Advances in Finite Element Analysis in Fluid Dynamics 1991, ASME FED-Vol. 123, December 1991, pp. 77-86.

[9] Heider R., Duboue J. M., Petot B., Billonnet G., Couaillier V., Liamis N.: *Three-dimensional analysis of turbine rotor flow including tip clearance*, ASME Paper 93-GT-111, 1993.

[10] Kang S., Hirsch C.: *Numerical simulation of three-dimensional viscous flow in a linear compressor cascade with tip clearance*, ASME Journal of Turbomachinery, Vol. 118, July 1996, 492-505.

[11] Koch C. C. : *Stalling pressure rise capability of axial flow compressor stages*, ASME Journal of Engineering for Power, Vol. 103, October 1981, 645-656.

[12] Launder B. E., Spalding D. B.: *The numerical computation of turbulent flows*, Computer Methods Appl. Mech. Eng., 3, 1974, 269-289.

[13] Merz P., Krückels J., Mayer J. F., Stetter H. : *Influence of grid refinement on the solution of the three-dimensional Navier-Stokes equations for flow in a transonic turbine stage with tip gap*, VDI Berichte Nr. 1185, 1995, 211-224.

[14] Pouagare M., Delaney R. A.: *Study of three-dimensional viscous flows in an axial compressor cascade including tip leakage effects using a SIMPLE-based algorithm*, ASME Paper 86-GT-84, 1986.

[15] Sjolander S. A., Amrud K. K.: *Effects of tip clearance on blade loading in a planar cascade of turbine blades*, ASME Journal of Turbomachinery, Vol. 109, April 1987, 237-245.

[16] Traupel W.: *Thermische Turbomaschinen-Erster Band*, Springer, 1977, 266 ff.

[17] Trenker M.: *Berechnung der ebenen turbulenten Strömung in einem NACA 65-Verdichtergitter*, Diplomarbeit, TU-Wien, 1997.

[18] Watanabe T., Nozaki O., Kikuchi K., Tamura A.: *Numerical simulations of the flow through cascades with tip clearance*, ASME FED-Vol.120, 1991, 131-139.

[19] Willinger R., Haselbacher H.: *Berechnung und Messung der ebenen turbulenten Strömung in einem geraden Turbinengitter*, Vortrag am FIDAP-Benutzertreffen, 23. und 24. Oktober 1996, Wiesbaden.

[20] Willinger R.: *Beitrag zur aerodynamischen Wechselwirkung zwischen axialer Turbinenstufe und nachgeschaltetem Diffusor*, Dissertation, TU-Wien, Jänner 1997.

[21] Willinger R., Haselbacher H.: *Experimental and numerical investigation of the secondary flow field in a linear turbine cascade*, Conference: Heat Engines and Environmental Protection, Tata, Hungary, May 25-28. 1997.

Badania eksperymentalne i numeryczne pola przepływu w liniowej kaskadzie turbiny przy uwzględnieniu efektów luzu wierzchołkowego

Streszczenie

Artykuł prezentuje badania trójwymiarowego pola przepływu w liniowej kaskadzie turbiny ze szczeliną wierzchołkową. Geometria kaskady odpowiada części wierzchołkowej poruszającego się układu łopatkowego turbiny gazowej nowoczesnej konstrukcji. Pięć szczelin wierzchołkowych, wliczając w to szczelinę o szerokości zero, przebadano eksperymentalnie. Sonda ciśnieniowa z pięcioma otworami przemieszczana była tuż za płaszczyzną krawędzi spływu. Wyniki eksperymentu wskazują na obecność upływowego wiru wierzchołkowego. Dalsza praca związana była z obliczeniami numerycznymi pola przepływu przez kaskadę przy użyciu solwera równań Naviera-Stokesa, w oparciu o metodę elementów skończonych. Modelowanie przepływu turbulentnego przeprowadzono przy pomocy modelu k - ε. Warunki brzegowe na wlocie, tzn. wartości średnie oraz turbulentne, przyjęto w oparciu o zmierzone pole prędkości na wlocie. Metoda obliczeniowa jest w stanie przewidzieć jakościowo najważniejsze cechy trójwymiarowego pola przepływu.